Scalar gradient and small-scale structure in turbulent premixed combustion

By S. H. Kim AND H. Pitsch

1. Motivation and objectives

The scalar gradient is a key quantity in describing and modeling turbulent mixing and combustion. In studies of scalar fields for non-reacting flows, it has been shown that the gradient of a passive scalar tends to align with the most compressive strain and that its magnitude is highly intermittent (Ashurst *et al.* 1987; Brethouwer *et al.* 2003; Warhaft 2000). As compared with the non-reacting case, the statistical characteristics of the gradient of a reactive scalar are not well understood due to the complexity in nonlinear turbulence/chemistry interaction. In chemically reacting flows, chemical reactions, the rate of which is influenced by turbulence, can have leading-order effects on the scalar gradient evolution, and the interaction of the scalar and turbulence fields can be strongly affected by thermal expansion due to heat release (Swaminathan & Grout 2006).

The characteristics of the scalar gradient in turbulent premixed flames are quite different from those in conserved scalar mixing. The evolution of scalar gradient fields for high Damköhler number (Da) flames (Damköhler 1940) is governed by strong coupling of diffusion and chemical reactions in relatively thin flame fronts, while, in non-reacting flows, turbulent straining is the unique mechanism of generating small-scale scalar variations. For the corrugated flamelet regime, where the thickness of the flame front is smaller than all turbulence length scales, the laminar flamelet theory well describes the structure of local flame fronts (Peters 2000), and the scalar gradient in turbulent flames is expected to be similar to that in corresponding laminar flames. However, the small-scale structure inside flame fronts is not fully understood for the moderate and low Da regime, such as the thin reaction zones regime or the broken reaction zones regime (Peters 2000), where the scale separation is not strictly valid.

The scalar gradient and flame broadening have been a subject of experimental and computational studies of premixed flames, especially with high turbulence intensity. While increasing turbulence intensity is generally expected to result in flame broadening, there has been controversy in the literature whether turbulence makes flame fronts thinner or thicker. The thickening of flame fronts has been reported by O'Young & Bilger (1997) and Chen & Mansour (1998), while the increase of the scalar gradient has been observed in other experiments (Buchsman *et al.* 1996; Soika *et al.* 1998) and direct numerical simulations (DNS) (Swaminathan & Bilger 2001). The importance of the Markstein number in flame thickening in the thin reaction zones regime has been proposed on the basis of the laminar flamelet theory (de Goey *et al.* 2005), while Law *et al.* (1994) and Sung *et al.* (1996) reported the insensitivity of the flame thickness to the flame stretch in their analysis of strained laminar flames. In general, large-scale turbulence contributes to flame thinning via a straining velocity field, while small-scale turbulence thickens flame fronts. The thickening process may depend on the relative importance of the effects of the large- and small-scale turbulence (de Goey *et al.* 2005). The curvature of flame fronts (Soika *et al.* 1998; Renou *et al.* 1998) and thermal expansion due to heat release are

also expected to have significant effects on the local turbulent velocity field and flame thickening/thinning processes. However, detailed physical mechanisms for flame thickening/thinning, and their relative importance have not been fully understood.

In this paper, we investigate the scalar gradient and the small-scale structure of turbulent premixed flames with emphasis on flame thickening/thinning. The Lagrangian equation for the evolution of the scalar gradient following an isoscalar surface is presented, which is useful in studying physical mechanisms for the scalar gradient evolution in propagating reaction front problems. The terms in the Lagrangian form of the scalar gradient equation are analyzed using DNS data for statistically 1-D planar flames with high intensity turbulence. Emphasized in this paper are the following: detailed mechanisms for flame thickening/thinning, the alignment of flame normal with turbulent strain, and the effects of heat release on these processes.

2. The equation for scalar gradients on isoscalar surfaces

In turbulent premixed flames, relatively thin reaction fronts propagate into turbulent medium, and the scalar gradient maintains itself due to the balance between diffusion and reactions. In this reaction front propagating problem, the Lagrangian-type equation is useful in studying the evolution of the local instantaneous reaction front structure. Of particular interest here is the time evolution of the scalar gradient following the flame surface.

The equation for a scalar ϕ can be written as

$$\frac{D\phi}{Dt} = (\mathbf{n}\cdot\mathbf{u}_\phi)|\nabla\phi| = \Omega_\phi, \tag{2.1}$$

where $\mathbf{u}_\phi$ is the velocity of the iso-surface relative to the fluid. $\frac{Dg}{Dt} = \frac{\partial g}{\partial t} + \mathbf{U}\cdot\nabla g$ is the Stokes derivative, where $\mathbf{U}$ is the fluid velocity. The normal vector $\mathbf{n}$ is defined as

$$\mathbf{n} = -\frac{\nabla\phi}{|\nabla\phi|}\,. \tag{2.2}$$

For a reacting scalar obeying Fickian diffusion, $\Omega_\phi = 1/\rho\nabla\cdot(\rho D\nabla\phi) + \omega_\phi$, where D is the molecular diffusivity, ω_ϕ is the chemical reaction rate, and ρ is the density. The displacement speed can be written as

$$u_\phi = \frac{1}{\rho|\nabla\phi|}\left[\nabla\cdot(\rho D\nabla\phi) + \omega_\phi\right]. \tag{2.3}$$

Taking the gradient of eqrefphieq and the inner product with $-\mathbf{n}$, we obtain

$$\frac{Dg}{Dt} = -\frac{1}{g}\nabla\phi\cdot\mathbf{S}\cdot\nabla\phi - \mathbf{n}\cdot\nabla\Omega_\phi, \tag{2.4}$$

where $|\nabla\phi| \equiv g$. $\mathbf{S}$ is a strain rate tensor defined by $1/2(\nabla\mathbf{U} + \nabla\mathbf{U}^T)$. The equation for the evolution of g following the iso-ϕ surface can be written as

$$\frac{D_\phi g}{Dt} = -g\mathbf{n}\cdot\mathbf{S}\cdot\mathbf{n} - g\mathbf{n}\cdot\nabla u_\phi, \tag{2.5}$$

where $\frac{D_\phi g}{Dt} = \frac{\partial g}{\partial t} + (\mathbf{U}+\mathbf{u}_\phi)\cdot\nabla g$. This equation can be rewritten as

$$\rho\frac{D_\phi g}{Dt} = -\rho g\mathbf{n}\cdot\hat{\mathbf{S}}\cdot\mathbf{n} - [\rho g\nabla\cdot\mathbf{U} - g u_\phi\mathbf{n}\cdot\nabla\rho] - g\mathbf{n}\cdot\nabla\rho u_\phi, \tag{2.6}$$

where $\hat{\mathbf{S}} = \mathbf{S} - (\nabla \cdot \mathbf{U})\mathbf{I}$. $\mathbf{I}$ is the identity matrix. From the continuity equation, we have

$$\frac{D_\phi \rho}{Dt} = -\rho \nabla \cdot \mathbf{U} + u_\phi \mathbf{n} \cdot \nabla \rho. \tag{2.7}$$

The equation for the normalized increase of the norm of the scalar gradient can therefore be written as

$$\frac{1}{g}\frac{D_\phi g}{Dt} = -\mathbf{n} \cdot \hat{\mathbf{S}} \cdot \mathbf{n} + \frac{1}{\rho}\frac{D_\phi \rho}{Dt} - \frac{1}{\rho}\mathbf{n} \cdot \nabla \rho u_\phi. \tag{2.8}$$

Note that each term on the right-hand side (r.h.s.) of the above equation vanishes in an unstretched laminar premixed flame. Decomposing the diffusion term in the displacement speed into the components normal and tangential to the isosurface, the displacement speed can be written as

$$u_\phi = -D\kappa + u_\phi^n, \tag{2.9}$$

where

$$u_\phi^n = \frac{1}{\rho|\nabla \phi|}\left[\frac{\partial}{\partial n}\left(\rho D \frac{\partial \phi}{\partial n}\right) + \rho \omega_\phi\right]. \tag{2.10}$$

$\kappa = \nabla \cdot \mathbf{n}$ is the mean curvature. κ is positive when an iso-scalar surface is convex toward the unburned side. n denotes the coordinate along the normal direction $\mathbf{n}$. With this decomposition, (2.8) can be rewritten as

$$\frac{1}{g}\frac{D_\phi g}{Dt} = -\mathbf{n} \cdot \hat{\mathbf{S}} \cdot \mathbf{n} + \frac{1}{\rho}\frac{D_\phi \rho}{Dt} - \frac{1}{\rho}\mathbf{n} \cdot \left[-\nabla(\rho D \kappa) + \nabla(\rho u_\phi^n)\right]. \tag{2.11}$$

By taking conditional averaging we obtain

$$\begin{aligned}\left\langle \frac{1}{g}\frac{D_\phi g}{Dt} | \phi = \varphi \right\rangle = \langle -\mathbf{n} \cdot \hat{\mathbf{S}} \cdot \mathbf{n} | \phi = \varphi \rangle + \left\langle \frac{1}{\rho}\frac{D_\phi \rho}{Dt} | \phi = \varphi \right\rangle \\ + \left\langle \frac{1}{\rho}\mathbf{n} \cdot \nabla(\rho D \kappa) | \phi = \varphi \right\rangle - \left\langle \frac{1}{\rho}\mathbf{n} \cdot \nabla \rho u_\phi^n | \phi = \varphi \right\rangle,\end{aligned} \tag{2.12}$$

where the angular brackets denote ensemble averaging conditioned on the quantity on the right side of the vertical bar.

It is worthwhile to review the physical meaning of the first term on the r.h.s. of (2.8). We have

$$\mathbf{n} \cdot \mathbf{S} \cdot \mathbf{n} = \mathbf{n} \cdot \nabla(\mathbf{U} \cdot \mathbf{n}) = \frac{\partial U_n}{\partial n}. \tag{2.13}$$

The first term on the r.h.s. of (2.8) is thus the dilatation on the tangential plane of an iso-ϕ surface, the so-called tangential strain rate:

$$-\mathbf{n} \cdot \hat{\mathbf{S}} \cdot \mathbf{n} = \nabla_T \cdot \mathbf{U}_T, \tag{2.14}$$

where ∇_T and $\mathbf{U}_T$ are the gradient operator and the velocity projected on the tangential plane, respectively. This represents the increase of surface area due to turbulent stretching (Chung & Law 1986; Candel & Poinsot 1990). For non-reacting scalar mixing in incompressible flows, the scalar gradient is aligned with the most compressive strain. Then, the average tangential strain is positive, and the area of a non-propagating surface increases (Batchelor 1954; Cocke 1963). For a propagating surface, the evolution of the surface area is also influenced by the curvature of the surface (Pope 1988; Chung & Law 1986; Candel & Poinsot 1990). The alignment characteristics are represented by the eigen-decomposition of the rate-of-strain tensor $\mathbf{S}$. Using the eigen-decomposition, the

tangential strain rate can be written as

$$-\mathbf{n}\cdot\hat{\mathbf{S}}\cdot\mathbf{n} = -[(\alpha_1-\Delta)\psi_1^2 + (\alpha_2-\Delta)\psi_2^2 + (\alpha_3-\Delta)\psi_3^2]. \tag{2.15}$$

α_i is the eigenvalue of the strain rate tensor $\mathbf{S}$, which satisfies $\alpha_1 \geq \alpha_2 \geq \alpha_3$ and $\alpha_1+\alpha_2+\alpha_3 = \Delta$. $\psi_i = \mathbf{n}\cdot\mathbf{e}_i$, where $\mathbf{e}_i$ is the eigenvector corresponding to α_i. The eigenvectors of $\hat{\mathbf{S}}$ are the same as those of $\mathbf{S}$. Hereafter, the tangential strain rate term is denoted by T_{ts}.

The second term on the r.h.s. of (2.8) represents the effects of the time evolution of the density along the trajectory of the iso-surface. In flames with unity Lewis number, this term represents compressibility effects and thus is negligible for low Mach number flows. This term also represents the effects of differential diffusion. In flames with non-unity Lewis number, the iso-surface of the progress variable can propagate with different speed from that of the density, even for the low Mach number limit. Hereafter, this term is denoted by T_ρ.

The last term of (2.8) represents the effects of variations of the mass flux along the normal to the iso-surfaces. In stationary laminar flames, we obtain

$$0 = -\mathbf{n}\cdot\hat{\mathbf{S}}\cdot\mathbf{n} - \frac{1}{\rho}\mathbf{n}\cdot\nabla\rho u_\phi. \tag{2.16}$$

This means that the mass flux through an isosurface varies in a straining velocity field. The variation can be estimated as

$$\frac{|\delta(\rho u_\phi)|}{\rho_u s_L} \sim \frac{l_F}{s_L}\frac{\rho|\hat{\mathbf{S}}|}{\rho_u} \sim \mathrm{Ka}, \tag{2.17}$$

where Ka is the Karlovitz number (Peters 2000), ρ_u is the density of the unburned gas, and s_L is the laminar flame speed. In the laminar flamelet regime with $\mathrm{Ka} \ll 1$, the variation will be negligible. In a highly strained flame with high Ka, the variation of the mass flux can be significant. In turbulent flames with moderate and low Da, e.g., those in the thin reaction zone regime, the small-scale wrinkling of flame fronts is significant such that the radius of curvature is of the order of thickness of an unstretched laminar flame. In that case, the radius of curvature can have significant variations for different iso-surfaces, which results in variations of the propagation speed. The curvature variation term, the third term on the r.h.s. of (2.11), emphasizes the role of the small-scale turbulence in turbulent mixing and flame thickening. The term involving u_ϕ^n represents the tendency to return to the unstretched laminar flame structure. Hereafter, the term involving κ and that involving u_ϕ^n are referred as the curvature variation term T_κ and the normal mass flux variation term T_n, respectively.

3. Direct numerical simulations

The compressible Navier-Stokes equations are solved:

$$\frac{\partial\rho}{\partial t} + \frac{\partial\rho u_j}{\partial x_j} = 0 \tag{3.1}$$

$$\frac{\partial\rho u_i}{\partial t} + \frac{\partial}{\partial x_j}(\rho u_i u_j) = -\frac{\partial p}{\partial x_i} + \frac{\partial\tau_{ij}}{\partial x_j} + \rho f_i \tag{3.2}$$

$$\frac{\partial\rho e}{\partial t} + \frac{\partial}{\partial x_j}[(\rho e + p)u_j] = \frac{\partial u_j\tau_{ij}}{\partial x_i} + \frac{\partial}{\partial x_j}\left(\lambda\frac{\partial T}{\partial x_j}\right) + \rho Q\omega_\phi \tag{3.3}$$

	u'/s_L	l/l_F	Da	Ka	Re_λ
PF1	13.8	3.9	0.28	14	95
PF2	19.5	2.75	0.14	28	95

TABLE 1. Characteristics of the simulated premixed flames (u': r.m.s. initial turbulent velocity, l: initial integral length scale, S_L: laminar flame speed, l_F: flame thickness based on the maximum temperature gradient, Da= $S_L l/(u' l_F)$, Ka= $D_u^2/(S_L l_K)^2$, l_K: Kolmogorov length scale, D_u: unburned mixture diffusivity, Re_λ: Reynolds number based on the Taylor scale).

$$\frac{\partial \rho\phi}{\partial t} + \frac{\partial}{\partial x_j}\left(\rho u_j \phi\right) = \frac{\partial}{\partial x_j}(\rho D \frac{\partial \phi}{\partial x_j}) + \rho\omega_\phi, \tag{3.4}$$

where

$$\rho e = \frac{1}{2}\rho u_j u_j + \frac{p}{\gamma - 1} \tag{3.5}$$

$$\tau_{ij} = \mu\left(\frac{\partial u_i}{\partial x_j} + \frac{\partial u_j}{\partial x_i} - \frac{2}{3}\delta_{ij}\frac{\partial u_k}{\partial x_k}\right). \tag{3.6}$$

p is pressure, e is the total internal energy, ω_ϕ is the chemical reaction rate of the scalar ϕ, Q is a heat release parameter. The thermal conductivity λ and the diffusion coefficient D are given as

$$\lambda = \mu c_p/Pr \text{ and } D = \mu/(\rho Sc), \tag{3.7}$$

where c_p is the specific heat at constant pressure. The dynamic viscosity μ is given as

$$\mu = \mu_u (T/T_u)^{0.7}. \tag{3.8}$$

The Prandtl number Pr and the Schmidt number Sc are set to 0.7. The gas mixture is assumed to be a perfect gas with a specific heat ratio of γ=1.4. The Mach number based on the root mean square (r.m.s.) velocity fluctuations is below 0.1 for all the cases studied here. The equations are integrated using a low-storage fourth-order Runge-Kutta method with a sixth order compact finite difference scheme for spatial discretization (Kennedy *et al.* 2000; Lele 1992).

The simulated flames are statistically 1-D premixed flames propagating in decaying homogeneous turbulence. The reaction rate is given by

$$\omega_{Y_R} = A Y_R \exp\left(-\frac{T_a}{T}\right), \tag{3.9}$$

where Y_R is the mass fraction of the deficient species in the reactant. The activation temperature T_a is set to be $4T_b$, where T_b is the burned gas temperature. The heat release parameter Q is chosen such that the density ratio between unburned and burned gas, γ, is equal to 6. The reaction progress variable is defined here as $C = 1 - Y_R/Y_{R,u}$, where the subscript u denotes the unburned side.

A non-reflecting boundary condition is used for the x_1 direction, while the x_2 and x_3 directions are periodic (Poinsot & Lele 1992). The equations are solved on 512×256×256 grid points. Initial turbulence is homogeneous and isotropic. The characteristics of the premixed flames are shown in Table 1. The initial turbulence intensity u'/s_L is larger than 10, while the length scale ratio l/l_F is approximately 3–4. The laminar flame thickness l_F is based on the maximum temperature gradient. The initial Da for the cases PF1 and PF2 are 0.14 and 0.28, respectively.

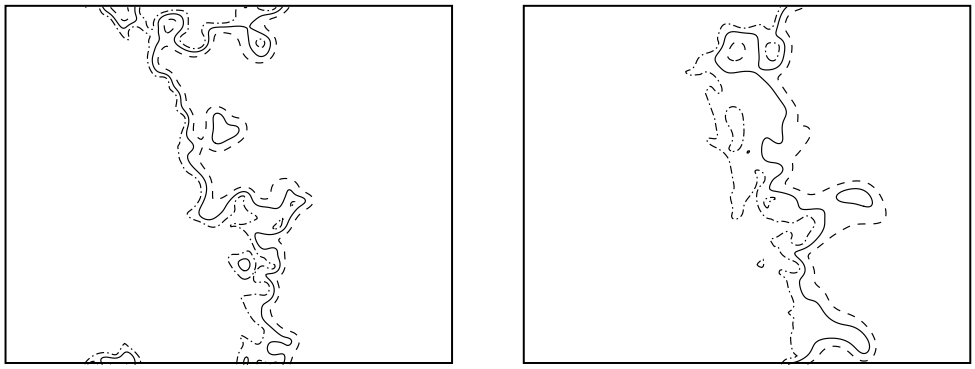

(a) (b)

FIGURE 1. Instantaneous fields of the reaction progress variable C for (a) PF1 and (b) PF2 (dashed dotted line: $C = 0.1$, solid line: $C = 0.5$, dashed line: $C = 0.9$).

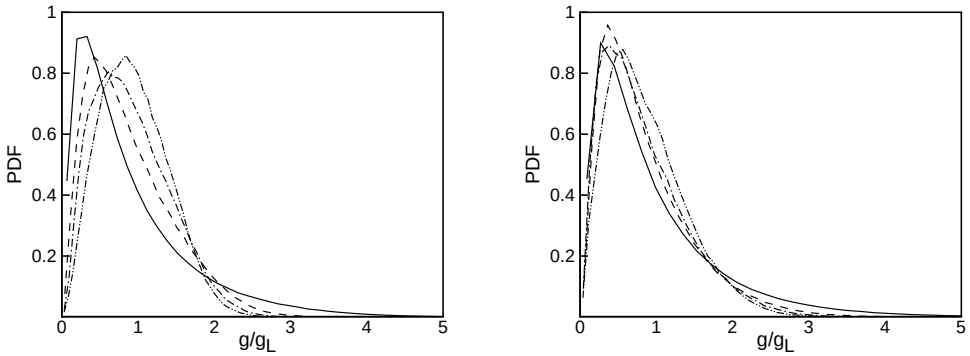

(a) (b)

FIGURE 2. PDFs of the normalized scalar gradient conditioned on $C = \zeta$ for (a) PF1 and (b) PF2 (solid line: $\zeta = 0.03$, dashed line: $\zeta = 0.08$, dashed dotted line: $\zeta = 0.13$, dashed dotted dotted line: $\zeta = 0.18$).

4. Results and discussion

4.1. *Characteristics of flame and scalar gradient field*

Figure 1 shows the instantaneous C-field for PF1 and PF2 at $\tau \approx 4.5$, where τ is the time normalized by the initial eddy turnover time l/u'. There is significant small-scale wrinkling as well as large-scale wrinkling for both cases. In the region with large curvature, where the small-scale turbulence is intense, the preheat zone is thickened. Variations of the curvature along the flame normal are also evident near this region. For PF2, flame thickening is more evident while, in some regions, thin flame fronts are also observed.

Figure 2(a) shows the conditional probability density function (PDF) of different nor-

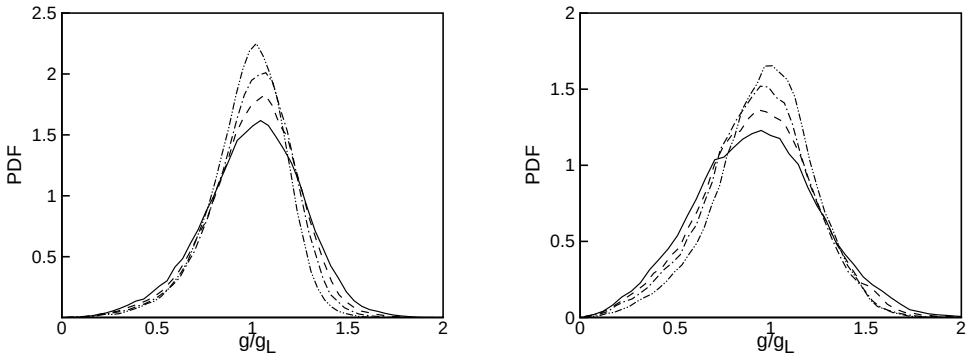

(a) (b)

FIGURE 3. PDFs of the normalized scalar gradient conditioned on $C = \zeta$ for (a) PF1 and (b) PF2 (solid line: $\zeta = 0.43$, dashed line: $\zeta = 0.48$, dashed dotted line: $\zeta = 0.53$, dashed dotted dotted line: $\zeta = 0.58$).

malized scalar gradients for $C < 0.2$ for PF1. For low values of C, the PDF is skewed with the peak at $g/g_L < 1$. While the preheat zone is thickened on average, the local scalar gradient can be significantly higher than the corresponding laminar flame value g_L. The conditional PDF for PF2 is shown in Fig. 2(b). For the lower Da case, the shift of the peak of PDF toward the higher g/g_L occurs more slowly with increasing C, which indicates that the flame is more broadened at these values, and has a wider distribution than that for PF1. The conditional PDFs for $0.45 < C < 0.65$ are shown in Fig. 3. For $0.45 < C < 0.65$, the PDF peaks around $g/g_L \sim 1$. The variance of the PDF becomes smaller as C increases. The conditional average of g is similar to the corresponding laminar value g_L.

4.2. *Balance of terms in the scalar gradient equation*

The terms in the scalar gradient equation are evaluated and shown in Fig. 4. The terms are averaged over the whole domain with the condition that $C = \zeta$, where ζ is the sample space variable of C. The balance of the terms for PF1 at $\tau \approx 2.5$ are shown in Fig. 4(a). On average, the local flame fronts are being thickened in the preheat zone. The conditional average of the normalized Lagrangian time derivative of g, $\langle 1/gDg/Dt|_\phi|\zeta\rangle$, is almost zero for $C > 0.5$, which indicates that there is no significant variation of the average flame thickness in the reaction zone. For PF1, there is a significant change in flame thickening processes in the preheat zone and the reaction zone. The balance of the terms for PF2 at $\tau \approx 2.5$ are shown in Fig. 4(b). For the lower Da case, the reaction zone as well as the preheat zone are being thickened. The conditional average $\langle 1/gD_\phi g/Dt|\zeta\rangle$ shows almost linear dependence on ζ, which indicates decreasing strength of the thickening processes with increasing ζ. The balance of the terms at a later time $\tau \approx 4.5$ for PF1 is shown in Fig. 4(c). The dependence of the average time derivative of g on ζ is qualitatively the same as that in Fig. 4(b), but the magnitude of each term is decreased due to decaying turbulence. As shown in Fig. 4(d), for PF2, the strength of the thickening process in the reaction zone is reduced more rapidly than that in the preheat zone. The terms on the r.h.s. of (2.11) show the same qualitative behavior for all plots shown in Fig. 4. The

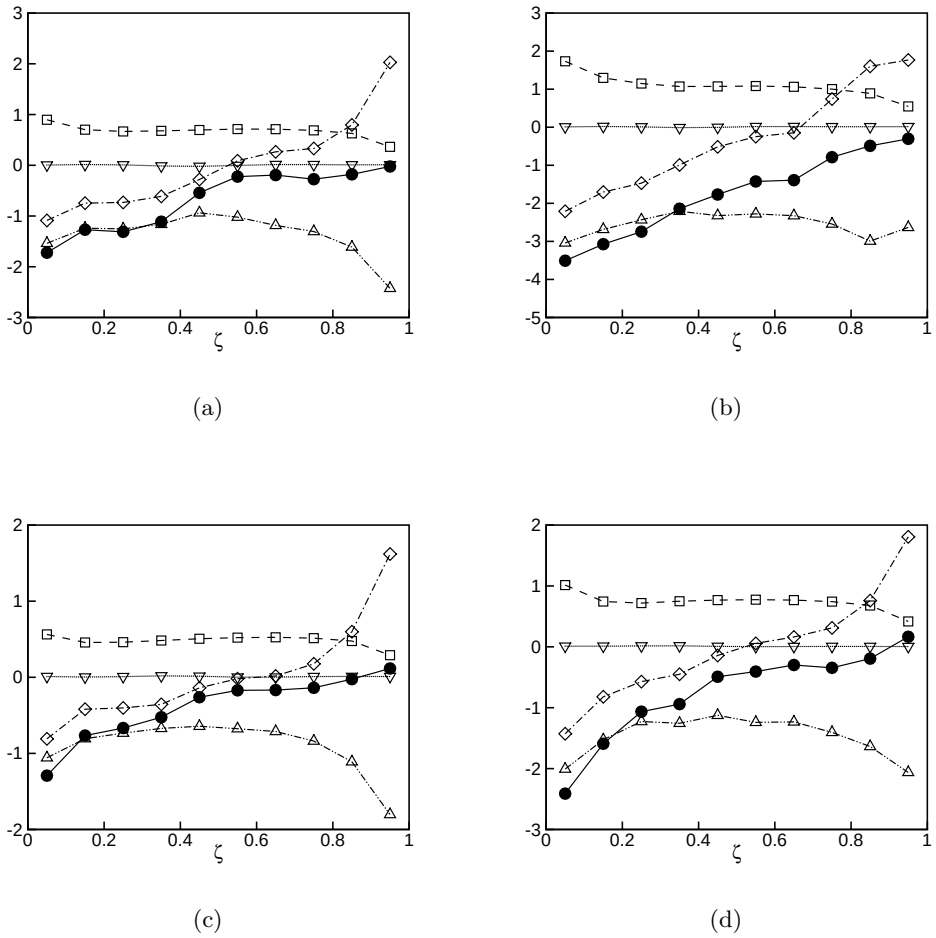

FIGURE 4. Balance of terms for (a) PF1 at $\tau = 2.5$, (b) PF1 at $\tau \approx 4.5$, (c) PF2 at $\tau \approx 2.5$ and (d) PF1 at $\tau \approx 4.5$ (squares: tangential strain rate term $\langle T_{ts}|\zeta\rangle$, upside down triangles: Lagrangian time derivative of the density $\langle T_\rho|\zeta\rangle$, diamonds: normal mass flux variation term $\langle T_n|\zeta\rangle$, triangles: curvature variation term $\langle T_\kappa|\zeta\rangle$, filled circles: $\langle 1/gD_\phi g/Dt|\zeta\rangle$; terms are normalized by the flame time scale t_F).

tangential strain rate term T_{ts}, which represents the turbulent stretching of the isoscalar surface, is a primary source of the scalar gradient generation. The curvature variations tend to thicken the flame fronts throughout. The major sink term in the scalar gradient equation is the curvature variation term T_κ in Fig. 4. The density variation term T_ρ is negligible in the present unity Lewis number flames. In the preheat zone, T_{ts} is balanced primarily with the normal mass flux variation term T_n, and the average time derivative $\langle 1/gD_\phi g/Dt|\zeta\rangle$ is almost equal to the curvature variation term T_κ. On the other hand, for $0.5 < C < 0.8$ with significant reaction rates, T_n does not contribute to flame thickening in the present flames. $\langle T_n|\zeta\rangle$ increases with ζ, and is balanced primarily with $\langle T_\kappa|\zeta\rangle$ for $\zeta \approx 1$.

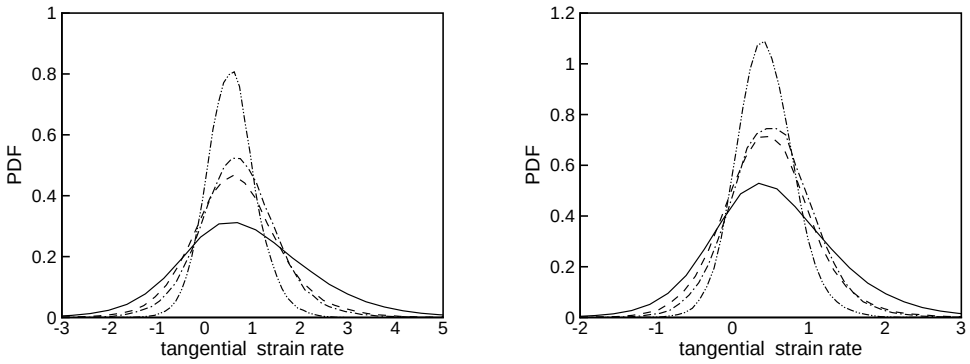

(a) (b)

FIGURE 5. PDFs of the tangential strain rate term T_{ts} conditioned on $C = \zeta$ at (a) $\tau \approx 2.5$ and (b) $\tau \approx 4.5$ (solid line: $\zeta = 0.03$, dashed line: $\zeta = 0.28$, dashed dotted line: $\zeta = 0.53$, dashed dotted dotted line: $\zeta = 0.93$; PF1).

4.3. *Tangential strain rate term and alignment characteristics*

Figure 5(a) shows the PDFs of the tangential strain rate term T_{ts} conditioned on $C = \zeta$ for PF1 at $\tau \approx 2.5$. The PDF is close to Gaussian with the peak at the positive value. As shown in Fig. 4, the conditional average $\langle T_{ts}|\zeta\rangle$ is positive for the whole range of ζ. This is consistent with the conjecture of Batchelor (1952). The positivity of the average stretching rate has been rigorously proven in an incompressible and isotropic field (Cocke 1969). Note that the variance becomes smaller with increasing ζ. This suggests the intensity of the small-scale turbulence becomes weaker when going to the burned side, as expected. The PDFs of T_{ts} at a later time $\tau \approx 4.5$ are shown in Fig. 5(b). While the level of the variance is reduced, the decreasing rate of the variance with ζ is similar to that at $\tau \approx 2.5$.

Figure 6 shows the joint PDF of the curvature κ and the tangential strain rate term T_{ts} for PF1 at $\tau \approx 4.5$. For the ensemble with $0.4 < C < 0.8$, T_{ts} has a negative correlation with the κ. The negative correlation has been observed previously in DNS (Chakraborty & Cant 2005) and in experiments (Soika *et al.* 1998). The correlation for the ensemble with $0.05 < C < 0.15$ is much weaker than that with $0.4 < C < 0.8$.

The correlation of the tangential strain rate and the curvature can be explained by the following decomposition of the tangential strain rate:

$$T_{ts} = -\mathbf{n} \cdot \check{\mathbf{S}} \cdot \mathbf{n} + \frac{2}{3}\Delta, \tag{4.1}$$

where

$$\check{\mathbf{S}} = \mathbf{S} - \frac{1}{3}\Delta\mathbf{I}. \tag{4.2}$$

In the first term on the r.h.s. of (4.1), the first-order effects of the dilatation is removed in the sense that the trace of the tensor $\check{\mathbf{S}}$ vanishes. The joint PDF of the curvature κ and the dilatation Δ is shown in Fig. 7. The dilatation shows a strong negative correlation with the curvature for the ensemble with $0.4 < C < 0.8$ in Fig. 7(b). The correlation becomes weaker for low values of C in Fig. 7(a). For the ensemble with $0.4 < C < 0.8$,

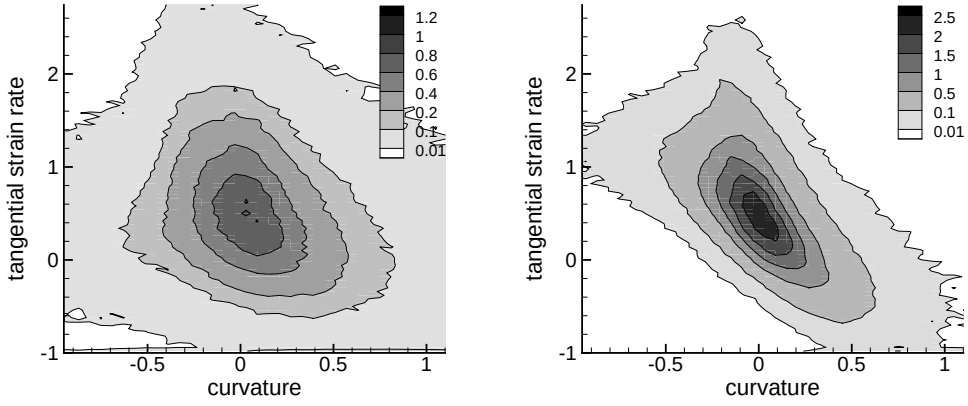

(a) (b)

FIGURE 6. The joint PDFs of the curvature and the tangential strain rate term for (a) the ensemble with $0.05 < C < 0.15$ and (b) the ensemble with $0.4 < C < 0.8$ (PF1, $\tau \approx 4.5$).

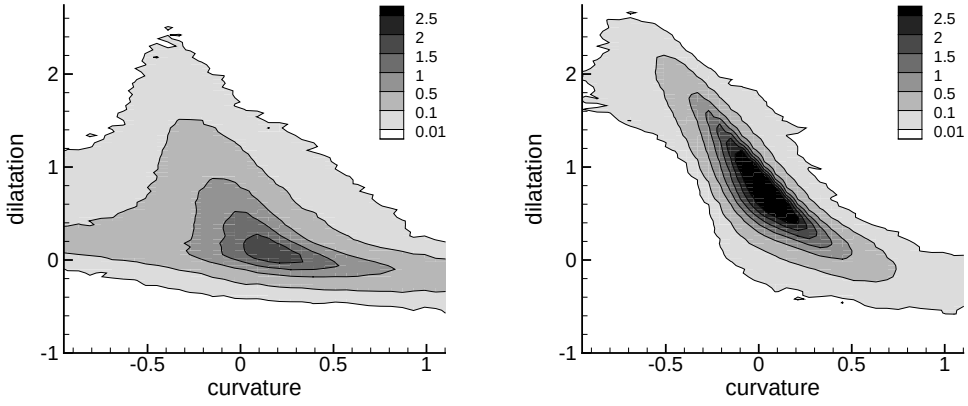

(a) (b)

FIGURE 7. The joint PDFs of the curvature and the tangential strain rate term for (a) the ensemble with $0.05 < C < 0.15$ and (b) the ensemble with $0.4 < C < 0.8$ (PF1, $\tau \approx 4.5$).

the slope of the conditional dilatation as a function of the curvature is steeper than that of the tangential strain rate by a factor of approximately 1.5, as indicated in (4.1). The conditional dilatation is known to be important in the structure of turbulent premixed flames (Swaminathan *et al.* 1997). In a flame with unity Lewis number and low Mach

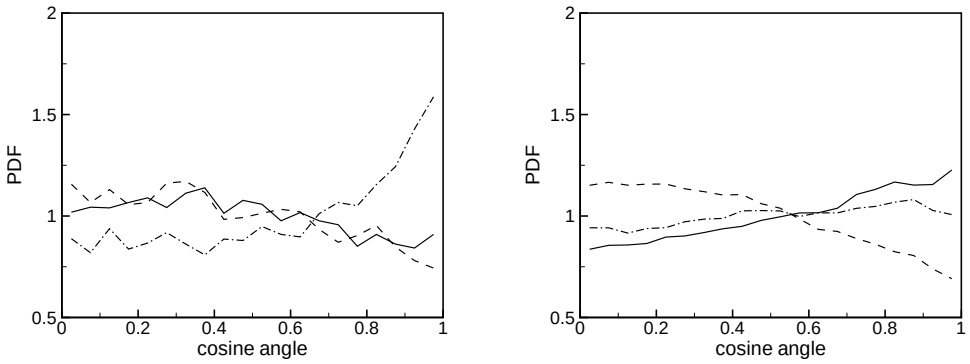

(a) (b)

FIGURE 8. PDFs of the cosine angle, ψ_i, between the flame normal $\mathbf{n}$ and the principal axis of the strain tensor, conditioned on (a) $\kappa = -0.5$ and (b) $\kappa = 0$, for the ensemble with $0.4 < C < 0.8$ (dashed dotted line: ψ_1, dashed line: ψ_2, solid line: ψ_3; PF1; $\tau \approx 4.5$).

number, the dilatation can be written as

$$\Delta = \frac{\beta}{\rho_u}(\nabla \cdot \rho D \nabla C + \rho \omega_C) = \beta g \frac{\rho u_C}{\rho_u} = \beta g \frac{1}{\rho_u}(\rho u_C^n - \rho D \kappa), \tag{4.3}$$

where $\beta = (T_b - T_u)/T_u$. (4.3) shows that the dilatation is closely related to the propagation property of the flame front. The dependence of the tangential strain rate on the curvature is mainly determined by the curvature dependence of the displacement speed, while the correlation with the scalar gradient can be of significance. As in the above equation, the displacement speed u_C has a negative correlation with the curvature κ.

In Figs. 6 and 7, the tangential strain rate is more scattered than the dilatation especially for the negative curvature, and the conditional average $\langle T_{ts}|\zeta\rangle$ is lower than $\langle \Delta|\zeta\rangle$ for large $|\kappa|$. These can be explained by investigating the alignment characteristics of the flame normal $\mathbf{n}$ with the principal axis of the strain. Figure 8 shows the PDF of the cosine angle, ψ_i, between the iso-surface normal vector $\mathbf{n}$ and the eigenvector of the strain rate tensor $\mathbf{e}_i$, conditioned on the curvature κ. PDF is evaluated for the ensemble with $0.4 < C < 0.8$. For $\kappa = -0.5$, which is normalized by s_L/D_u, the normal vector $\mathbf{n}$ is more aligned with the most extensive strain. Considering that the eigenvectors of $\check{\mathbf{S}}$ are the same as those of $\mathbf{S}$ and that the trace of $\check{\mathbf{S}}$ is equal to zero, the term, $-\mathbf{n} \cdot \check{\mathbf{S}} \cdot \mathbf{n}$, becomes negative, and therefore contributes in the opposite direction to the dilatation term. Turbulent fluctuations of this term are responsible for the weaker correlation between T_{ts} and κ. In Fig. 8, $\mathbf{n}$ has no evident preferential alignment for very low values of $|\kappa|$, while the PDF for ψ_3 is slightly higher than those for ψ_2 and ψ_3 near $\psi_i = 1$. Overall, the term $-\mathbf{n} \cdot \check{\mathbf{S}} \cdot \mathbf{n}$ tends to reduce the scalar gradient for large $|\kappa|$ in the present flame.

To further investigate the alignment characteristics, the PDFs of ψ_i conditioned on $C = \zeta$ are shown in Fig. 9. For low and high values of ζ, the scalar gradient is more aligned with the most compressive strain, but the degree of the alignment is not as strong as in conserved scalar mixing (Asherst *et al.* 1987). No preferential alignment of the scalar gradient is observed in the middle of the flame front, while the PDF of ψ_i is

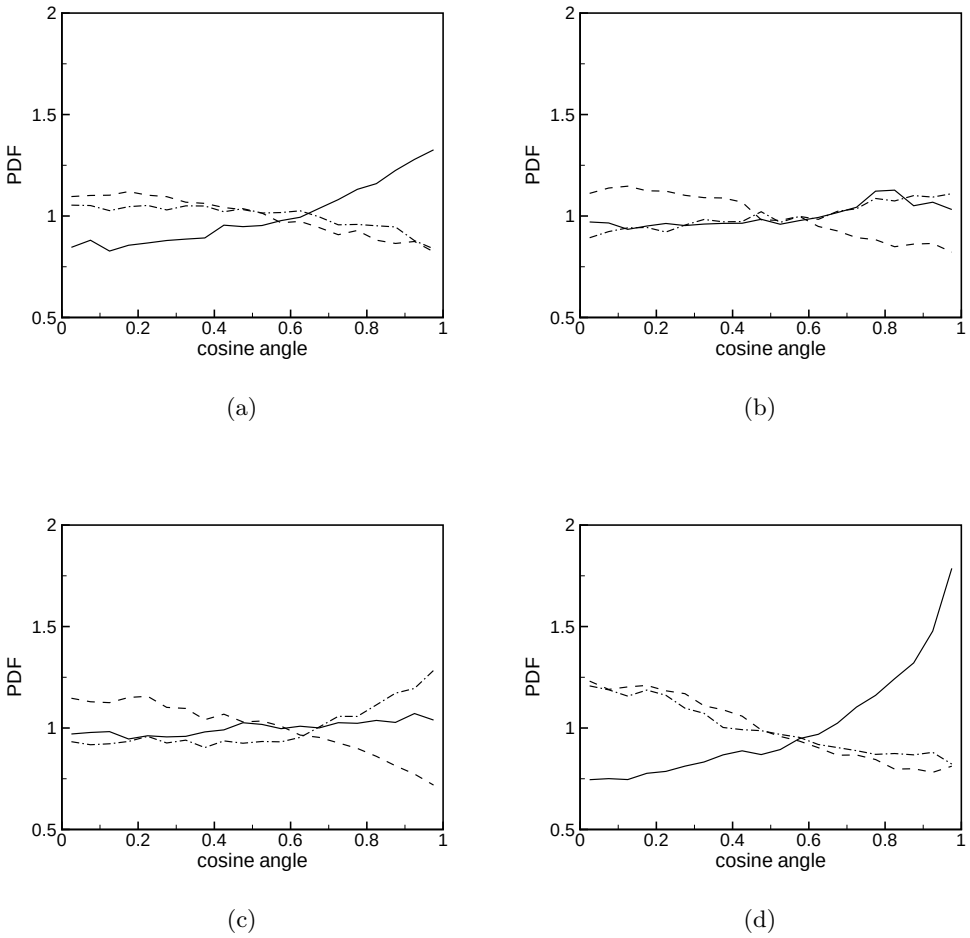

FIGURE 9. Alignment characteristics on iso-scalar surfaces with (a) $C = 0.05$, (b) $C = 0.25$, (c) $C = 0.55$, and (d) $C = 0.95$ (dashed dotted line: ψ_1, dashed line: ψ_2, solid line: ψ_3; PF1; $\tau \approx 4.5$).

slightly higher than others in Fig. 9(c). For $\zeta = 0.6$, the dilatational velocity induced by the heat release is largest.

As shown in Figs. 8 and 9, the alignment characteristics in premixed flames are significantly different from those in non-reacting flows, due to the heat release effects and the different origin of the generation mechanism of the scalar gradient. In their study of the alignment characteristics in turbulent premixed flames with high Da, Swaminathan & Grout (2006) found that the scalar gradient in high Da premixed flames aligns with the most extensive strain in contrast to non-reacting scalars. This is because in high Da flames the velocity field induced by heat release is dominant over the turbulent velocity field. The dilatational velocity is mostly in the flame normal direction in high Da flames. In non-reacting flows, the preferential alignment of the scalar gradient with the most compressive strain has been reported (Ashurst *et al.* 1987; Warhaft 2000). The present

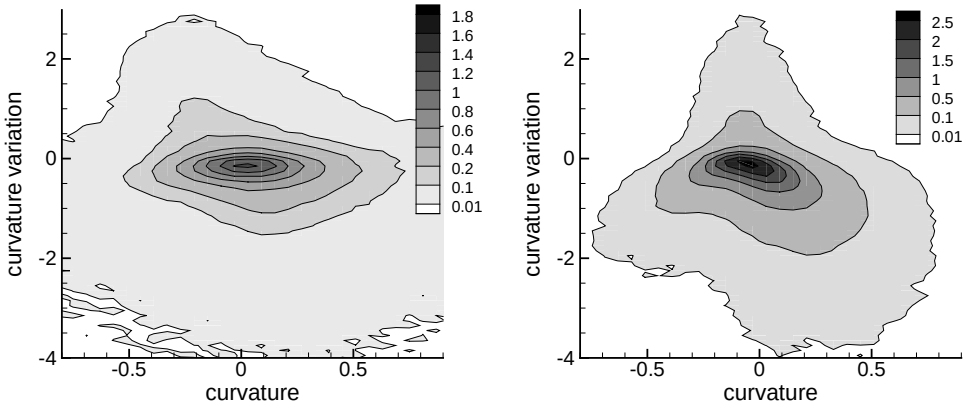

FIGURE 10. The joint PDFs of the curvature and the curvature variation term for (a) the ensemble with $0.05 < C < 0.15$ and (b) the ensemble with $0.4 < C < 0.8$ (PF1, $\tau \approx 4.5$).

results show that the alignment of the scalar gradient with the most extensive strain rate becomes less evident with decreasing Da. Alignment characteristics are determined by the relative importance of the dilatation and the turbulence. Since the dilatation is of the order of β/τ_c, where τ_c is the chemical time scale, and the strain rate is of the order of the small-scale turbulent time scales, the relative importance of the dilatation can be estimated by the parameter β/Ka. The dependence of the aligment characteristics on ζ is primarily due to that of the dilatation on ζ. In addition, due to the correlation between the dilatation and the curvature, the alignment characteristics in premixed flames show stronger dependence on the curvature than in non-reacting scalars.

The dependence of the tangential strain rate on the curvature is a direct consequence of the heat release effects in premixed flames. The relationship between the dilatation and the displacement speed is primarily responsible for this dependency. In reaction front propagation with no heat release, such dependence of the tangential strain rate on the curvature will not be observed. It is expected that, in the front with no heat release, the tangential strain rate has a maximum near $\kappa = 0$ and decreases with increasing $|\kappa|$.

4.4. *Effects of the tangential strain rate and the curvature on the mass flux variation term*

Figure 10 shows the joint PDF of the curvature κ and the curvature variation term T_κ for PF1. T_κ has a negative correlation with the $|\kappa|$ for the ensemble with $0.4 < C < 0.8$. This implies that smaller-scale wrinkling is more responsible for flame thickening. T_κ always has a negative value when $|\kappa|$ is large. For low values of $|\kappa|$, T_κ can be positive, while it is much more probable for T_κ to be negative. For large $|\kappa|$, the wrinkling is of the order of the flame thickness and significant variations of the curvature across flame fronts occur. T_κ then plays a key role in the thickening of flame fronts. Significant scattering in the joint PDF means the importance of small-scale turbulence that can locally make high curvature and associated curvature variation near the iso-surface with small curvature. As shown in Fig. 11(b), T_κ has essentially no correlation with the curvature for the

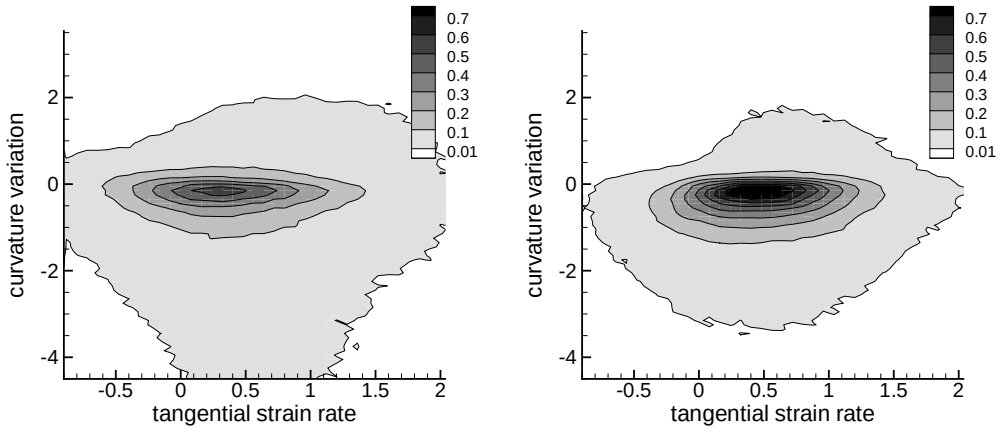

FIGURE 11. The joint PDFs of the tangential strain rate and the curvature variation term for (a) the ensemble with $0.05 < C < 0.15$ and (b) the ensemble with $0.4 < C < 0.8$ (PF1, $\tau \approx 4.5$).

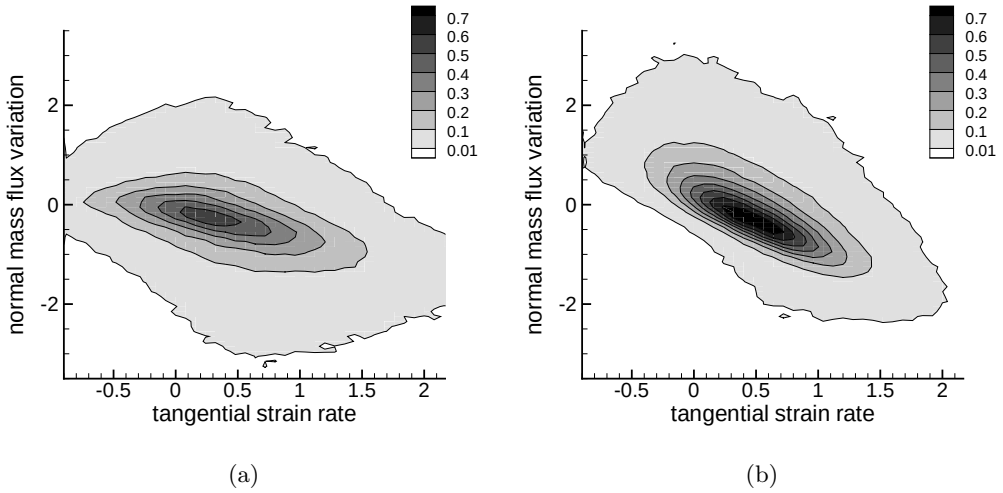

FIGURE 12. The joint PDFs of the tangential strain rate and the normal mass flux variation term for (a) the ensemble with $0.05 < C < 0.15$ and (b) the ensemble with $0.4 < C < 0.8$ (PF1, $\tau \approx 4.5$).

ensemble with $0.5 < C < 0.15$. The response of the reaction fronts to wrinkling is different for different iso-surfaces, while the curvature variations contribute to reduce the scalar gradient for all ranges of C. The curvature variation term has no correlation with the tangential strain rate term in Fig. 11.

Figure 12 shows the joint PDF of the tangential strain rate term T_{ts} and the normal mass flux variation term T_n for PF1. T_n has a negative correlation with T_{ts} for both

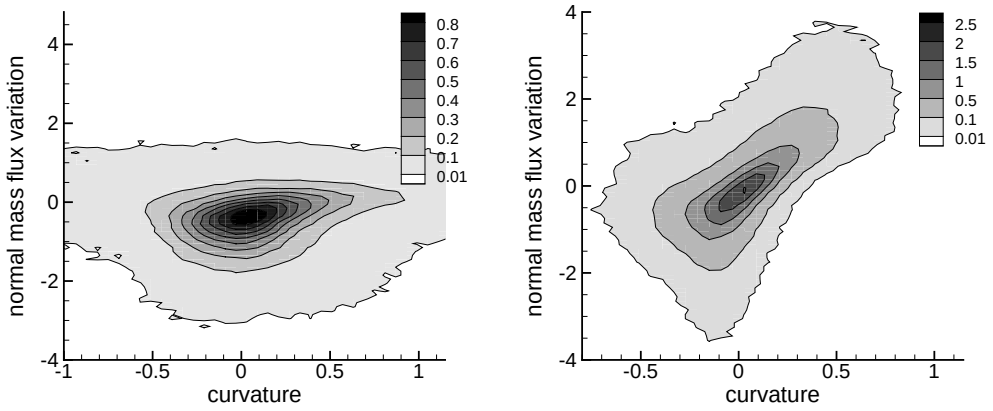

(a) (b)

FIGURE 13. The joint PDFs of the curvature and the normal mass flux variation term for (a) the ensemble with $0.05 < C < 0.15$ and (b) the ensemble with $0.4 < C < 0.8$ (PF1, $\tau \approx 4.5$).

ensemble with $0.05 < C < 0.15$ and that with $0.4 < C < 0.8$. This correlation is determined by the response of the unstretched flame to the straining velocity field. For the preheat zone with no reaction, the normal mass flux term has the contribution only from diffusion normal to the iso-surface, and the positive tangential strain rate enhances the normal diffusion, which reduces the scalar gradient. The same argument applies to the reaction zone, since the reaction rate on an iso-surface does not change for unity Lewis number. In Fig. 12(b), T_κ has a negative correlation with the tangential strain rate. This can be explained by (2.16).

Figure 13 shows the joint PDF of the curvature κ and the normal mass flux variation term T_n. For the ensemble with $0.4 < C < 0.8$, T_n has a positive correlation with the κ, but the correlation is weaker than that between the tangential strain rateT_{ts} and the normal mass flux T_n. This correlation does not indicate the direct influence of κ on the normal mass flux variations, but comes from the correlation between κ and T_{ts}. The correlation between κ and T_n for the ensemble with $0.4 < C < 0.8$ is weaker than that with $0.4 < C < 0.8$.

5. Conclusion

The scalar gradient and the small-scale structure of turbulent premixed flames with high turbulence intensity are investigated using DNS data for statistically 1-D planar flames. The evolution equation for the scalar gradient following an iso-scalar surface is presented. In the Lagrangian form of the scalar gradient equation, which is useful in propagating reaction front problems, the evolution of the scalar gradient on an iso-scalar surface is governed by the tangential strain rate, the Lagrangian time derivative of the density, and the mass flux variations along the normal to the iso-scalar surface. The mass flux variation term is decomposed into the normal and the tangential components to investigate the effects of the curvature.

The major sink term in the scalar gradient equation is shown to be the curvature

variation term, while the tangential strain rate term is a major source term. In the preheat zone, the average of the tangential strain rate term conditioned on the progress variable is balanced with that of the normal mass flux variation term, and the conditional average Lagrangian time derivative of the scalar gradient is approximately equal to the conditional average curvature variation term. In the reaction zone, the curvature variation term is primarily balanced with the tangential strain rate term. It is observed that the thickening process in the reaction zone is much weaker than that in the preheat zone. In one of our simulated flames, a sudden drop of the strength of flame thickening in the reaction zone was observed.

The statistics of each term in the scalar gradient equation are investigated. The tangential strain rate and the curvature are found to have a negative correlation. It is shown that the negative correlation is due to the relation between the dilatation and the displacement speed of an iso-scalar surface. This implies that the heat release effects are of significant importance in the evolution of the scalar gradient in premixed flames. The dependence of the dilatation on the curvature is also shown to affect the alignment characteristics of the flame normal with the principal axis of the strain. The curvature variation term is found to have a negative correlation with the magnitude of the curvature, which suggests that smaller-scale wrinkling is more responsible for flame thickening.

REFERENCES

Ashurst, Wm. T., Kerstein, A. R., Kerr, R. M. & Gibson, C. H. 1987 Alignment of vorticity and scalar gradient with strain rate in simulated Navier-Stokes turbulence. *Phys. Fluids* **30**, 2343–2353.

Batchelor, G. K. 1952 The effect of homogeneous turbulence on material lines and surfaces.*Proc. Royal Soc. London* **A213**, 349–366.

Brethouwer, G., Hunt, J. C. R. & Nieuwstadt, F. T. M. 2003 Micro-structure and Lagrangian statistics of the sclar field with a mean gradient in isotropic turbulence. *J. Fluid Mech.* **474**, 193–225.

Candel, S. M. & Poinsot, T. J. 1990 Flame stretch and the balance equation for flame area. *Combust. Sci. Tech.* **70**, 1–15.

Chen, Y. C. & Mansour, M. S. 1998 Investigation of flame broadening in turbulent premixed flames in the thin-reaction-zones regime. *Proc. Combust. Inst.* **28**, 811–818.

Chakraborty, N. & Cant, R. S. 2005 Effects of strain rate and curvature on surface density function transport in turbulent premixed flames in the thin reaction zone regime. *Phys. Fluids* **17**, 065108.

Chung, S. H. & Law, C. K. 1984 An invariant derivation of flame stretch. *Comb. Flame* **55**, 123–125.

Cocke, W. J. 1969 Turbulent hydrodynamic line stretching: consequences of isotropy. *Phys. Fluids* **12**, 2488–2492.

Damköhler, G. 1940 Der einflußder Turbulenz auf die Flammengeschwidigkeit in Gasgemischen. *Z. Electrochem* **46**, 601–652.

de Goey, L. P. H., Plessing, T., Herrmanns, R. T. E. & Peters, N. 2005 Analysis of the flame thickness of turbulent flamelets in the thin reaction zones regime. *Proc. Combust. Inst.* **30**, 859–866.

Gibson, C. H. 1968 Fine structure of scalar fields mixed by turbulence. I. Zero-gradient points and minimal gradient surfaces. *Phys. Fluids* **11**, 2305–2315.

Kennedy, C. A., Carpenter, M. H. & Lewis, R. M. 2000 Low-storage, explicit Runge-Kutta schemes for the compressible Navier-Stokes equations. *Appl. Nume. Math.* **35**, 177–219.

Law, C. K., Sung, C. J., Yu, G. & Axelbaum, R. L. 1994 On the structural sensitivity of purely strained planar premixed flames to strain rate variations. *Comb. Flame* **98**, 139–154.

Lele, S. K. 1992 Compact finite difference schemes with spectral-like resolution. *J. Comp. Phys.* **103**, 16–42.

O'Young, F & Bilger, R. W. 1997 Scalar gradient and related quantities in turbulent premixed flames. *Comb. Flame* **109**, 682–700.

Peters, N., Terhoeven, P., Chen, J. H. & Echekki, T. 1998 Statistics of flame displacement speeds from 2D unsteady methane-air flames. *Proc. Combust. Inst.* **28** 833–839.

Peters, N. 2000 *Turbulent Combustion*, Cambridge University Press.

Poinsot, T. J. and Lele, S. K. 1992 Boundary conditions for direct numerical simulations of compressible viscous flows. *J. Comp. Phys.* **101**, 104–129.

Pope, S. B. 1988 The evolution of surfaces in turbulence. *Int. J. Eng. Sci.* **28**, 445–469.

Renou, B., Boukhalfa, A., Puechberty, D. & Trinité, M. 1998 Effects of stretch on the local structure of freely propagating premixed low-turbulent flames with various Lewis numbers. *Proc. Combust. Inst.* **27**, 841–847.

Soika, A., Dinkelacker, F & Leipertz, A. 1998 Measurement of the resolved flame structure of turbulent premixed flames with constant Reynolds number and varied stoichiometry. *Proc. Combust. Inst.* **27**, 785–792.

Sung, C. J., Liu, J. B. & Law, C. K. 1996 On the scalar structure of nonequidiffusive premixed flames in counterflow. *Comb. Flame* **106**, 168-183.

Swaminathan, N., Bilger, R. W. & Ruetsch, G. R. 1997 Interdependence of the instantaneous flame front structure and the overall scalar flux in turbulent premixed flames. *Combust. Sci. Tech.* **128**, 73–97.

Swaminathan, N. & Bilger, R. W. 2001 Scalar dissipation, diffusion and dilatation in turbulent H-2-air premixed flames with complex chemistry. *Combust. Theory Modelling.* **3**, 429–446.

Swaminathan, N. & Grout, R. W. 2006 Interaction of turbulence and scalar fields in premixed flames. *Phys. Fluids* **18**, 045102.

Warhaft, Z. 2000 Passive sclars in turbulent flows. *Annu. Rev. Fluid Mech.* **32**, 203–240.